18TH ESA SYMPOSIUM
ON EUROPEAN ROCKET AND BALLOON PROGRAMMES AND RELATED RESEARCH

3-7 JUNE 2007

VISBY SWEDEN

SECOND ANNOUNCEMENT
& CALL FOR PAPERS

esa

RYMDSTYRELSEN
Swedish National Space Board

Swedish Space Corporation

TRUE-2 MODULE ONBOARD MASER 10: TECHNICAL ACHIEVEMENTS AND SCIENTIFIC RESULTS.

F. Peluso, C. Albanese, M. Lappa, F.S. Gaeta

Microgravity Advanced Research and user Support Center – MARS srl
via E. Gianturco 31, 80146 Naples, ITALY, peluso@marscenter.it

ABSTRACT

The TRUE-2 module was the re-flight of a previous module, TRUE, Thermal Radiation Unsteady Experiment, flown onboard Maser 8 in 1999. Aim of the TRUE module was to detect and measure the forces produced by a temperature gradient crossing the interface between a solid body and a liquid in which it is immersed. These forces are named Thermal Radiation Forces (TRF) introduced and theorized by the Principal Investigator of the scientific team.

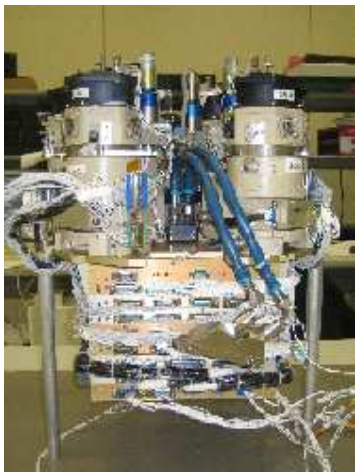

Figure 1. TRUE-2 module.

The experimental procedure foresaw the activation of two distinct thermal ramps; surprisingly, the second ramps generated a force signal higher than that generated by the first thermal wave front. This aspect has requested a deep analysis by the scientific team. Improved numerical simulations of the thermal field generated inside the cell and of the ensuing fluid motion induced by the residual gravity level have been used as a powerful tool for evaluating a variety of effects related to the application of the temperature gradient.

1. INTRODUCTION

Aim of the TRUE experiment is to measure the forces produced on a solid body immersed in a liquid and crossed by a flux of heat. These forces are called Thermal Radiation Forces (TRF) and, due to their smallness and strongly dependence upon the temperature gradient, their detection on ground on large objects is severely and adversely affected by buoyancy. The microgravity environment thus was selected and used as a more suitable condition for performing an experiment for detecting the TRFs.

The TRUE-2 module has flown onboard the Maser 10 mission, and was entirely realized by a team of Italian industries, MARS as prime, Techno-System Development and DTM technologies. The main upgrade with respect to the original TRUE module was the adoption of a properly designed and realized force sensor for the measurement of the very weak TR Forces. The sensor was provided by the Gibertini Elettronica, an Italian SE world leader in the field of precision electronic balances for laboratory use. The new sensor had the requested performances for the detection of the forces, and confirmed the right choice in the shape, geometry and characteristics of the force sensor. Indeed it allowed measuring the forces being immersed in the liquid samples, bypassing all the technical problems encountered with the sensor used for the first TRUE flight. An aspect to be improved was the coating of metallic parts of the sensor' chassis.

The re-flight of the TRUE-2 module was agreed by ESA since the maiden flight suffered of spurious accelerations induced by a centrifuge mounted in another module, which disturbed the measurement [1].

Figure 2. One of the TRUE-2 Cells

Totally six identical cells, labelled A to F, were installed on the module, shown in Fig. 1, five filled with pure water, one with glycol. One spare cell was assembled and taken ready in case of damaging of one of the cells mounted on the module. The solid body was a solid disc made of Plexiglas; for one of the five cells filled with water a double slab was mounted with the aim of measuring the delay in the force signal when crossing the two slabs. The scientific results of the

experiment confirmed the ambiguous and debated ones got after the TRUE maiden flight. Five of the six embarked experimental cells worked properly providing absolutely clearly discernable force signals synchronized with the two thermal ramps activated during the six minutes time laps of microgravity. Although an automatic sequence was foreseen for the entire execution of the experiments, some telecommands were sent from the Ground Control Center in Kiruna to recover one of the sensors which failed the "zero" position synchronization after the release of the launch fixations.
Unfortunately, due to the huge impact on ground, the TRUE-2 module h/w was completely damaged and is not re-usable.

2. THE FLIGHT CELLS.

The experimental cell, shown in Fig. 2, consists of a main body made of Peak, to which the force sensor is attached. Temperature sensors (thermistors) protruding into the cell for monitoring the liquid temperature close to the disc, a pressure sensor for revealing leakages, the electric pass-through for the force sensor and two filling valves are also mounted on the main body. A special blocking mechanism has been foreseen for preventing the mobile parts from damage at launch. This device is also mounted on the main body. The cover of the cell includes the low thermal inertia heater, related thermistors, and the bellow for compensating the liquid volume expansion. The heater, which was also designed for this application, is faced to the disc, about 1.5 mm apart, with the aim of generating the largest possible thermal gradient across it.

Cell	Slab	Liquid	Residual mass (g)	Conversion factor 1 dyne=(μA)
A	1	Water	0.250	1.480
B	1	Glycol	-0.0254	1.472
C	1	Water	0.436	1.467
D	2	Water	-0.432	1.474
E	1	Water	0.176	1.460
F	1	Water	0.313	1.471

Table 1.

Substance	K/u (cgs)
Water	0,41
Glycol	0,16
Plexiglas	0,06

Table 2.

As mentioned before, the force sensor, shown in Fig. 3, was suitably designed for this application with precise requirements, among them the sensitivity, readiness, liquid compatibility, movement along a single axis, fixed position during the measurement. Attached to the force sensor, a ballast provides the suitable buoyant force for minimising the residual mass of all moving parts. All the six ballasts had identical shape and volume; fine tuning of the ballast mass was made possible by adding small pieces of several dimensions and masses inside its empty volume. The final residual masses obtained after the fine-tuning for the six cells are listed in Tab. 1, where also the type of liquid and the number of discs are reported. The solid disc is eventually attached to the ballast by means of three titanium small shafts. For one of the cells filled with water, two adjacent slabs have been mounted, 1.0 mm apart. Slab dimensions are 50.0 mm in diameter, 0.5 mm thickness.

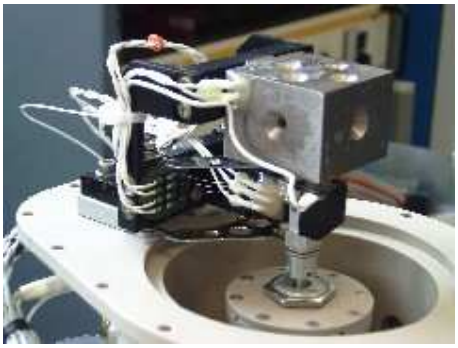

Figure 3. The force sensor installed into the cell.

3. THE PHYSICAL MODEL OF TRF

Let's consider a system in which the heat flows across a surface of discontinuity between two adjacent media, as two immiscible liquids or a solid and a liquid. The heat flux is continuous through the limiting surface, but there is a discontinuity in the momentum flux, due to the abrupt change of the propagation velocity of thermal waves - an extreme case of anharmonicity. A thermal radiation force is produced at the interface [2-6] given by:

$$F_{l,s}^{th} = \pi r_s^2 H_{l,s}\left[\left(\frac{K}{u}\right)_l - \left(\frac{K}{u}\right)_s\right]\left\langle\frac{dT}{dz}\right\rangle \qquad (1)$$

where suffixes l and s stand for liquid and solid phases respectively, K and u are the thermal conductivity and the speed of sound in the related materials, r is the radius of the solid material, and H is a numerical coefficient accounting for the reflection of acoustical waves at the interface. From the eq. (1), it is immediate to note the dependence of the TRF upon: the cross section of the obstacle, the temperature gradient, and the difference on the two ratios in square brackets. This last term provides the orientation to the vectorial force: if the numerical value of the ratio for the medium *l* is larger than for the medium *s*, then the force is directed along the temperature gradient; in the opposite case, the force will push the obstacle along the direction of the heat flux. For both the liquids used in the experiment, the expected direction of TRF is along the heat flux. Values of K/u ratio at T=20ºC for the three substances used are listed in Tab. 2.

4. THE FLIGHT EXPERIMENT.

The experimental sequence was entirely executed automatically. It was chosen with the main goal of performing two thermal ramps with the highest

possible efficiency. The sequence foresaw commands for mechanically unlocking the slabs (blocked at launch), activate the force sensors control, activate the thermal ramps with the predetermined time laps between them, lock again the slabs before re-entry. Telemetry data were sent to ground at 1Hz rate, and saved onboard at 10Hz rate.
Residual gravity acceleration was still present during the microgravity period, and precisely in the range between $-1.5\cdot10^{5}\,g_0$ and $+1.0\cdot10^{-6}\,g_0$ as from data provided by Swedish Space Corporation, shown in Fig.4, where data are expressed in units of millig.

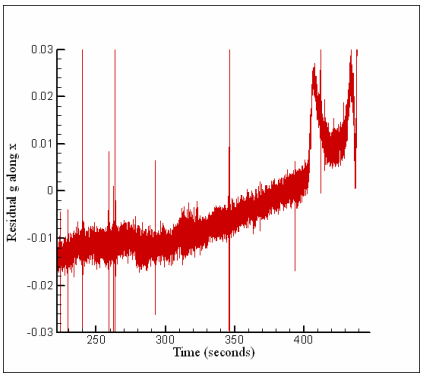

Figure 4. Residual g along the heat flux direction, expressed in units of millig. By courtesy SSC.

We have identified the following forces as certainly acting on the disc during the measurement: a) forces due to hydrodynamic disturbances and caused by the fluid movement, F^{hyd}; b) buoyancy forces due to the thermal expansion of liquid (we have neglected the thermal expansion of the solid parts), F_b^{th}; c) force due to the residual gravity acceleration and acting on the imbalanced mass of movable parts (see Tab.1), F^{b}; d) thermal radiation forces, due only to the heat flux, F^{th}. During the experiment all these forces acted all together on the disc. In order to discern the intensity and, in general, the role played by each of these contributions, accurate numerical simulations have been carried out and the TRF evaluated from their theoretical expression. Precisely, F^{hyd} is the integral over the disc surface of the pressure difference between the upper and lower disc surfaces induced by the fluid motion inside the cell. F_b^{th} is the volume integral over the portion of liquid exhibiting a temperature increase with respect to the initial one, settled at =20C. For the evaluation of the buoyancy experienced by the disc, both the actions due to the thermal heating and the effective residual gravity level have been taken into account. Finally, F^{b} has been calculated as given by the product of the residual mass (see Tab.1) times the effective residual g present during the experiment. F^{th} has been computed according to Eq. (1) and considering the actual temperature distribution around the disc.
We address the reader to the following section for additional details on such a model.

5. THE NUMERICAL MODEL

5.1 Governing equations and boundary conditions.

In the presence of steady acceleration levels the velocity and temperature fields related to the ensuing thermal buoyancy convection can be determined by solution of the differential balance equations (for mass, momentum, and energy).
Following the usual Boussinesq approximation for incompressible fluids, the physical properties have been assumed constant, except for the density ρ in the generation term in the momentum balance equation, which is assumed to be a linear function of temperature:

$$\rho = \rho_0 \left[1 - \beta_T (T - T_0)\right] \tag{2}$$

where β_T is the thermal expansion coefficients, and T_0 a reference value for the temperature (20C in this case). In other words, the continuity equation has been reduced to the vanishing of the divergence of the velocity field, and variations of the density have been ignored in the momentum equation, except insofar as they give rise to a gravitational force. The nondimensional form results from scaling the lengths by a reference distance (L) and the velocity $\underline{V}$ by the energy diffusion velocity $V_\alpha = \alpha / L$ (α is the thermal diffusivity); the scales for time t and pressure p are, respectively, L^2/α and $\rho_0 \alpha^2 / L^2$. The temperature, measured with respect to T_0, is scaled by ΔT. This approach leads to:

$$\underline{\nabla} \cdot \underline{V} = 0 \tag{3}$$

$$\frac{\partial \underline{V}}{\partial t} = -\underline{\nabla} p - \underline{\nabla} \cdot \left[\underline{V}\underline{V}\right] + \mathrm{Pr}\ \nabla^2 \underline{V} + \mathrm{Pr}\, Ra\, T\, \underline{i}_g \tag{4}$$

$$\frac{\partial T}{\partial t} = -\underline{\nabla} \cdot \left[\underline{V} T\right] + \nabla^2 T \tag{5}$$

and the relevant nondimensional numbers are the well-known Prandtl and Rayleigh numbers (Gr is the Grashof number):

$$\mathrm{Pr} = \frac{\nu}{\alpha} \tag{6a}$$

$$Gr = \frac{g \beta_T \Delta T L^3}{\nu^2} \tag{6b}$$

$$Ra = Gr\,\mathrm{Pr} = \frac{g \beta_T \Delta T L^3}{\nu \alpha} \tag{6c}$$

ν being the kinematic viscosity.

5.2 The numerical method.

According to the well-known SMAC method [7,8] the computation of the velocity field at each time step is

split into two substeps. In the first, an approximate non-solenoidal velocity field $\underline{V}^*$ which corresponds to the correct vorticity of the field is computed at time (n+1) neglecting the pressure gradient term in the momentum Eq. (4). In the second substep, the pressure field is computed by solving the equation resulting from the divergence of the momentum equation taking into account Eq. (3):

$$\nabla^2 p^n = \frac{1}{\Delta t}\underline{\nabla}\cdot\underline{V}^* \qquad (7)$$

On the physical boundaries the $\partial p/\partial n = 0$ condition is imposed. Finally, the correct solenoidal velocity field is updated using the computed pressure field to account for continuity:

$$\underline{V}^{n+1} = \underline{V}^* - \Delta t\underline{\nabla}p^n \qquad (8)$$

The temperature distribution at time (n+1) is obtained from Eq. (5) after the velocity calculation.

Validation of the present algorithm has been obtained through quantitative extensive comparison with other recent solutions available in the literature.

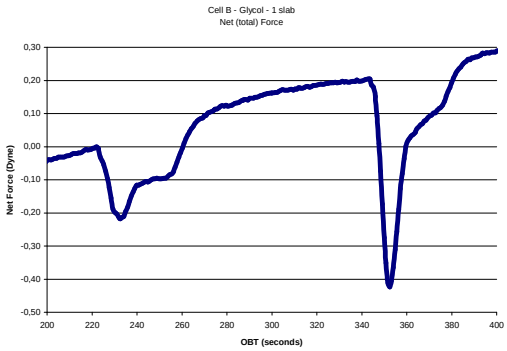

Figure 5. Plot of the total net force measured for Cell B

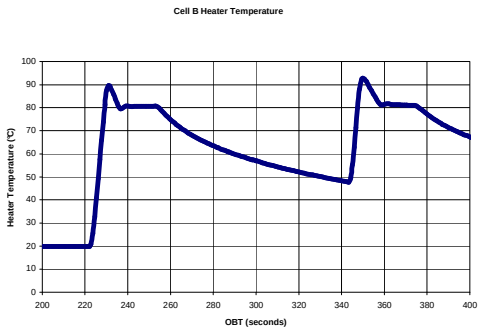

Figure 6. Plot of heater temperature for Cell B.

6. FLIGHT EXPERIMENT RESULTS.

Among the six cells mounted on the TRUE-2 module, four filled with water and the one filled with glycol worked perfectly, confirming the good design of the new force sensor. Cell A did not work properly, although a telecommand was successfully sent by the Kiruna base and acknowledged onboard. The other four cells filled with water provided signals of low intensity, synchronised with the thermal ramp. Cell B filled with Glycol provided an intense signal, clearly synchronised with the thermal ramps. Heaters worked nominally, with the foreseen performance. All thermistors were alive for all the duration of the experiment. No leakages were detected in the cells. Force signal of cell D did not reveal the expected "double signal" due to the presence of the double slab.

Besides cell B, because of the similarity of the forces measured from the four cells filled with water, in the following we will analyse in detail only Cell F, which showed the best signal-to-noise ratio. Plots of force measured with cell B and the heater temperature are shown in Figs. 5 and 6 respectively, where data are reported only for the time interval of interest. The same data for cell F are reported in Figs. 7 and 8. From the plots it is evident the synchronization of the force signal with the thermal ramps, the delay between the beginning of the thermal ramp and that of the force signal being about 0.1 second. Also evident is the higher intensity of the second force signal wrt the first, as well as its higher intensity for glycol than for water.

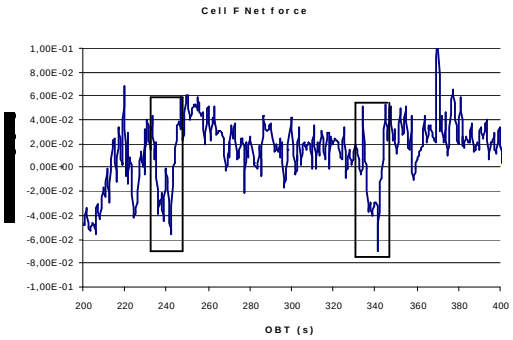

Figure 7. Plot of the total net force measured for Cell F

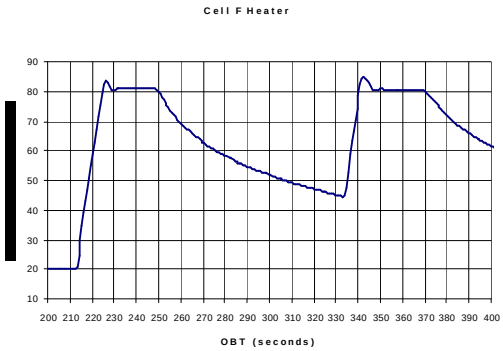

Figure 8. Plot of heater temperature for Cell F.

As explained before, the values of the several forces that contributed the total force measured have been evaluated along with the method described in section 4. For both liquids, the temperature and velocity fields have been numerically solved and plots are given in Figs. 9 and 10 for water and glycol respectively, and the several forces calculated, including the TRF. In both cases, the hydrodynamic force F^{hyd} represents a

negligible disturbance, amounting to $5 \cdot 10^{-11}$ dyne for glycol and $5 \cdot 10^{-10}$ dyne for water. The F_b^{th} provides a contribution slightly higher (but however well below the minimum sensitivity of the force sensor) amounting in the average to $-2 \cdot 10^{-5}$ dyne for water and $-5 \cdot 10^{-5}$ dyne for glycol. A contribution at the resolution limit of the force sensor is that of the residual gravity, F^b. It holds 10^{-3} dyne for water, and 10^{-4} dyne for glycol. The time dependence of the above forces, due to the variation with time of the residual g, has been also taken into account. TRF's on the contrary show two distinct peaks, corresponding to the two thermal ramps. For the first and second ramp they amount to –9 and –6 dyne for water, respectively, and to –1.7 and –1.12 dyne for glycol. Comparison between the (total) force signal measured in flight and the total force evaluated from numerical calculation, are plotted in Figs. 11 and 12 for water and glycol respectively.
In the case of water the calculated total force is some orders of magnitude larger than the measured force. Not the same in the case of glycol, where calculated and measured forces have comparable values.

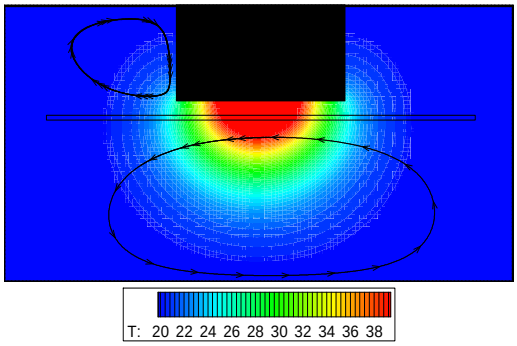

Figure 9. Temperature and velocity fields in water at the end of the second thermal ramp.

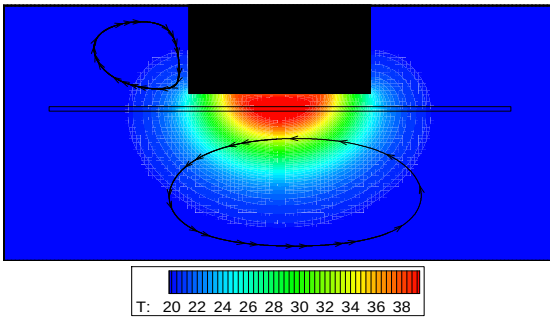

Figure 10. Same as in Figure 9, but for glycol.

7. DISCUSSION AND CONCLUSIONS.

7.1 Performances of the flight h/w.

As already pointed out at the beginning of the previous section, the performances of the flight h/w were absolutely satisfactory for all the subsystems, which brought to a general good performance of the TRUE-2 module. A special mention deserves the force sensor, which was designed and developed for this flight. The force sensor revealed the winning card for this kind of studies, opening probably new perspectives for those experiments, in microgravity environments, as well as for ground based laboratories, which need severe, accurate and sensitive devices for measuring weak forces, also if immersed in liquids.

7.2 Scientific results.

Forces measured in both liquids show some features that cannot be explained in terms of the spurious forces evaluated. The forces other than TRF's indeed all provide contributions that are negligible with respect to the TRF. This is confirmed by the plots shown in Figs. 13 and 14, for water and glycol respectively, where the total force measured is compared with the TRF deduced from flight data by subtracting all the evaluated contributions from the total measured force. It is evident that, for both water and glycol, the effect measured is absolutely not due to F^{hyd}, F_b^{th} and F^b; besides, the forces are clearly synchronised with the thermal ramps, and show a trend which is similar to the theoretical ones, shown in Figs. 10 and 11. The analysis of the results shows also forces having the foreseen direction with respect to that of the heat flux.
However, some discrepancies are also evident. The first which jumps to the eye is that the forces measured in water are much different from those expected, because they are not only lower than expected but also lower than those for glycol. Another, although less important particular is that for both liquids the force measured in correspondence of the second thermal ramp is larger than that corresponding to the first ramp. Since the temperature gradient generated from the first ramp is certainly larger that that generated from the second, because a larger part of the liquid is at the starting, cold temperature, the opposite response would be expected.
The discrepancies described above between the data obtained for glycol and those for water cannot be ascribed to an unexpected behaviour of the force sensors, because all of them in the four cells gave analogous results. Hence one should look for an explanation in the theoretical expression for TRF, reported in eq. (1). One can see that the force depends essentially on three factors, namely the temperature gradient, the difference in the two rations in square brackets, and the numerical term H. Among these, the second and the third are certainly those suffering the larger uncertainty in their evaluation, due to their strong dependence on the actual thermal profile. Another relevant aspect of these forces is that, despite of their simple expression, they are supposed to act at mesoscopic level [3,4,6], eq. (1) representing an expression tentatively applied on macroscopic systems. Having in mind this concept, one may argue that, while for glycol the values associated to the thermodynamic variables at macroscopic level are likely the same as at

mesoscopic level (Local Thermodynamic Equilibrium), the same does not holds for water, where mesoscopic values of thermodynamic and dynamic variables, such as K, u, ρ, T, are drastically different from those at macroscopic level. This confirm the peculiarity of water among the liquids existing in nature.

The *lesson learned* from this experiment is that in future possible experiments for measuring the TRF, besides the adoption of a similar force sensor, one should investigate the behaviour in several liquids, such for instance, silicon oils, glycerine, alcohols, etc., but except the water, to verify and confirm the very interesting results obtained for glycol in the TRUE-2 experiment.

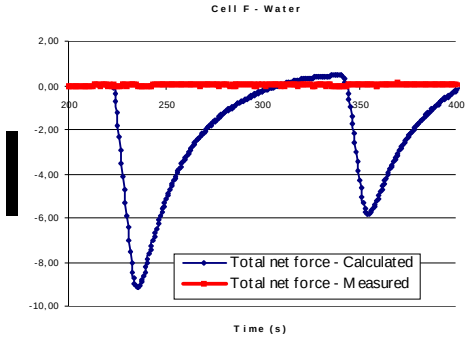

Figure 11. Plot of measured and calculated total forces for water.

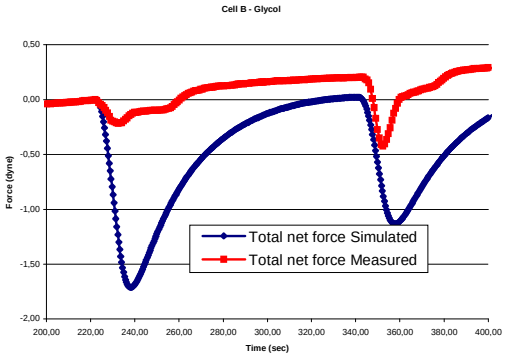

Figure 12. Plot of measured and calculated total forces for glycol.

8. ACKNOWLEDGEMENTS.

The PI of the TRUE-2 experiment is grateful to the industrial team, SSC, MARS, TS DEV, DTM and Gibertini Elettronica for the careful preparation of the flight experiment. A special mention is for the MARS personnel, which has provided the technical and scientific support during the flight campaign and in elaborating the flight data.

Special thanks are also for mr. W. Herfs, Prof. G. Frohberg and mr. K. Löth for their invaluable support.

The realization of this experiment was made possible thanks to the ESA financial support and technical management.

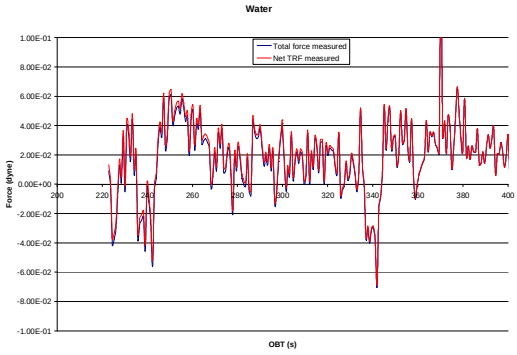

Figure 13. Plot of measured total force and of the TRF deduced along with equation (9) for water. The two curves are practically indistinguishable.

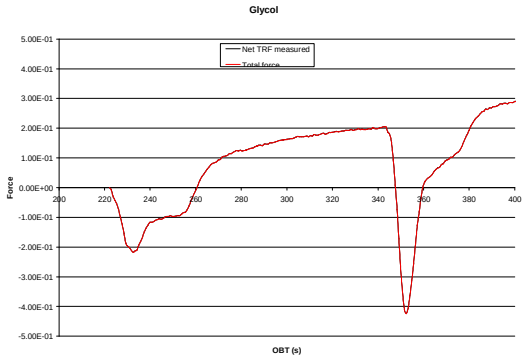

Figure 14. the same as Figure 13, but for glycol.

9. REFERENCES.

1. Albanese C., Peluso F., Gaeta, F.S., "Thermal Radiation Forces in microgravity: the TRUE Experiment results", *Microgravity and Space Station Utilization*, vol. 4/4, 2002.
2. Gaeta F.S., Ascolese E., Tomicki B., *Phys. Rev. A*, vol. 44, 5003, 1991.
3. Gaeta F.S., Peluso F., Mita D.G., Albanese C., Castagnolo D., *Phys. Rev E*, vol. 47, 1066, 1993.
4. Gaeta F.S., Albanese C., Mita D.G., Peluso F., *Phys. Rev E*, vol. 49, 433, 1994.
5. Albanese C., Dell'Aversana P., Gaeta F.S., *Phys. Rev. Letters*, vol. 79, 4151, 1997.
6. Gaeta F.S., Peluso F., Albanese C., Mita D.G., *Lecture Notes in Physics*, vol. 464, 221, 1995.
7. Lappa M., *Science and Supercomputing at CINECA*, vol. 11, 326-340, 1997.
8. Lappa M., *Microgravity and Space Station Utilization*, vol. 3 (4), 51-62, 2002.